A Generalised Signature Method for Multivariate Time Series Feature Extraction

James Morrill [1 2 *] **Adeline Fermanian** [3 *] **Patrick Kidger** [1 2 *] **Terry Lyons** [1 2]

Abstract

The 'signature method' refers to a collection of feature extraction techniques for multivariate time series, derived from the theory of controlled differential equations. There is a great deal of flexibility as to how this method can be applied. On the one hand, this flexibility allows the method to be tailored to specific problems, but on the other hand, can make precise application challenging. This paper makes two contributions. First, the variations on the signature method are unified into a general approach, the *generalised signature method*, of which previous variations are special cases. A primary aim of this unifying framework is to make the signature method more accessible to any machine learning practitioner, whereas it is now mostly used by specialists. Second, and within this framework, we derive a canonical collection of choices that provide a domain-agnostic starting point. We derive these choices as a result of an extensive empirical study on 26 datasets and go on to show competitive performance against current benchmarks for multivariate time series classification. Finally, to ease practical application, we make our techniques available as part of the open-source [redacted] project.

1. Introduction

A multivariate time series is obtained by observing d quantities evolving with time, which can be written as an array $\mathbf{x} = (x_1, \ldots, x_n)$, where n is the length of the series, and $x_i \in \mathbb{R}^d$ for each $i \in \{1, \ldots, n\}$. These data are common in various fields (finance, health, energy...) and offer several specific challenges: they are often highly dimensional, as both the number of channels d and the length of the series n may be large, the values x_i are correlated, and the different channels may interact. Finally, the inputs may be of different length and the data may be irregularly sampled.

One approach is to construct models that directly accept some of these issues; for example recurrent neural networks handle correlated inputs with varying lengths. A second option is to use feature extraction techniques, which normalise the data so that other techniques may then be applied. Methods such as the shapelet transform (Ye & Keogh, 2009; Grabocka et al., 2014; Kidger et al., 2020), Gaussian process adapters (Li & Marlin, 2016; Futoma et al., 2017; Moor et al., 2020), and in particular the signature method (Levin et al., 2013), all fit into this category.

The approach taken by the signature method, coming from rough path theory (Lyons et al., 2007; Friz & Victoir, 2010), is to interpret a multivariate time series as a discretisation of an underlying continuous path. The *signature transform*, also known as the *path signature* or *signature*, can then be applied, which produces a vector of real-valued features that are known to characterise the path.

Benefits of the signature method include: a high degree of flexibility, making it possible to customise the method to specific datasets; strong theoretical guarantees; an interpretable feature set; ease of handling irregularly sampled and/or partially observed data; and it being well-defined for some highly irregular processes such as ARMA, Gaussian processes or even Brownian motion. Also, signature features do not need to learned, which can make them particularly effective on (but not limited to) low sample datasets.

The flexibility of the signature method has made it possible to be tailored to specific applications and achieve state-of-the-art performance in wide range of problem domains, such as handwriting recognition (Wilson-Nunn et al., 2018; Yang et al., 2016b), action recognition (Yang et al., 2016a; 2017), and medical time series prediction tasks (Morrill et al., 2019; 2020b). However, this flexibility comes at the cost of additional complexity in the model search space.

---

*Equal contribution [1]Mathematical Institute, University of Oxford, UK [2]The Alan Turing Institute, British Library, UK [3]Sorbonne Université. Correspondence to: James Morrill <morrill@maths.ox.ac.uk>.
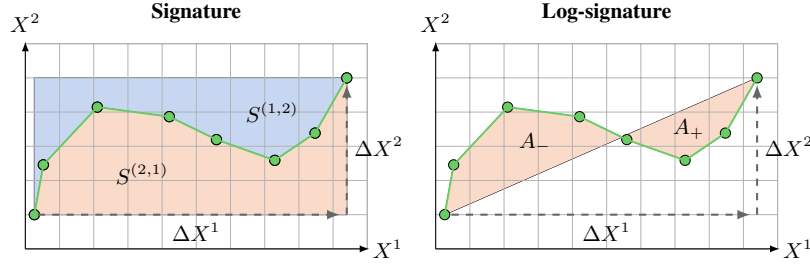
Figure 1. Geometric depiction of the depth-2 signature and log-signature. The depth-1 term of both transforms equate to the displacements of the path over the interval in each coordinate, these being $\Delta X^{1,2}$. **Left:** The signature. Depth-2 terms $S^{(1,2)}$, $S^{(2,1)}$ correspond to the areas of the blue and orange regions respectively. **Right:** The log-signature. Only one depth-2 term which is given by the signed area $A_+ - A_-$. This is known as the *Lévy area* of the path.

To the best of our knowledge, no comprehensive studies exist that collate and combine the most common method variations found in the literature and assemble them under a common mathematical framework. Additionally, no baseline signature model has ever been tested against other time series classification baselines. Our goal will be to address both of these issues, alongside the development of an open source implementation, so as to make the methods more accessible to a wider audience.

Contributions We introduce a *generalised signature method* that contains the many existing variations as special cases. In doing so we are able to understand their conceptual groupings into what we term *augmentations*, *windows*, *transforms* and *rescalings*. This involves a comprehensive review of the existing variations across the literature. By understanding their commonality, we are then able to combine different variations, and propose new options that fit into this framework.

We go on to examine which choices within this framework are most important to success by performing an extensive empirical study across 26 datasets. To the best of our knowledge this is the first study of this type.

In doing so, we are then able to produce a canonical signature pipeline. This represents a domain agnostic starting point that may then be adapted for the task at hand. We show that the performance of this canonical pipeline is comparable to current state-of-the-art classifiers for multivariate time series classification, including deep recurrent and convolutional neural networks. This has led to the implementation of this generalised approach in the open source [redacted] package.

2. Context

2.1. Background theory

We begin with a few mathematical definitions necessary throughout the article.

Definition 1. Let $d \in \mathbb{N}$, we denote the space of time series over $\mathbb{R}^d$ as

$$\mathcal{S}(\mathbb{R}^d) = \{(x_1, \ldots, x_n) \,|\, x_i \in \mathbb{R}^d, n \in \mathbb{N}, n \geq 1\}.$$

If $d = 1$, then $\mathbf{x}$ is a univariate time series, whereas if $d > 1$, $\mathbf{x}$ is a multivariate time series. Given $\mathbf{x} = (x_1, \ldots, x_n) \in \mathcal{S}(\mathbb{R}^d)$, n is called the length of $\mathbf{x}$ and d its dimension or number of channels. We assume that in addition to the array of values $\mathbf{x} \in \mathcal{S}(\mathbb{R}^d)$, we have access to a vector of increasing time stamps $\mathbf{t} = (t_1, \ldots, t_n)$. If the data is regularly sampled, then $\mathbf{t}$ can be set to $\mathbf{t} = (1, \ldots, n)$, which will often be the case.

We consider a *dataset* to be a collection of such samples. Note that the time stamps $\mathbf{t}$ for each sample may be different, and the sample lengths n can vary. That is, we accept varying length and irregular sampling without modification. We are now in a position to define the signature of a time series.

Definition 2. Let $\mathbf{x} \in \mathcal{S}(\mathbb{R}^d)$ and $\mathbf{t} = (t_1, \ldots, t_n)$ its associated timestamps. Let $X = (X_t^1, \ldots, X_t^d)_{t \in [t_1, t_n]}$ be a piecewise linear interpolation of $\mathbf{x}$ such that for any $i \in \{1, \ldots, n\}$, $X_{t_i} = x_i$. Then the depth-N signature transform of $\mathbf{x}$ is the vector defined by

$$
\begin{aligned}
\mathrm{Sig}^N(\mathbf{x}) = \big(&\{S(\mathbf{x})^{(i)}\}_{i=1}^d, \\
&\{S(\mathbf{x})^{(i,j)}\}_{i,j=1}^d, \\
&\ldots, \\
&\{S(\mathbf{x})^{(i_1,\ldots,i_N)}\}_{i_1,\ldots,i_N=1}^d\big) \in \mathbb{R}^{\frac{d^{N+1}-1}{d-1}}
\end{aligned}
$$

where for any $(i_1, \ldots, i_k) \in \{1, \ldots, d\}^k$,

$$S(\mathbf{x})^{(i_1,\ldots,i_k)} = \int \cdots \int_{t_1 \leq u_1 < \cdots < u_k \leq t_n} \mathrm{d}X_{u_1}^{i_1} \ldots \mathrm{d}X_{u_k}^{i_k} \in \mathbb{R}.$$

While this definition may seem somewhat technical, there are several intuitions that can be made with regard to the

signature features. We present a geometric interpretation of the first two levels of the signature and log-signature in Figure 1. The depth-1 terms, $S(\mathbf{x})^{(i)}$, equate to the displacement of the path over the interval in the ith coordinate, denoted by ΔX^i in Figure 1. The depth-2 terms, $S(\mathbf{x})^{(i,j)}$, have interpretations in areas generated over the interval.

From a statistical point of view, the signature can be thought of as the equivalent of a moment-generating function for time series. Let Z be a random variable, then the moment-generating function of Z is the function

$$t \mapsto \mathbb{E}[e^{tz}] = \sum_{k=0}^{\infty} \frac{t^k}{k!} \mathbb{E}[Z^k]$$

and, if well-defined, it characterizes the distribution of Z. Assume that X is a random time series (that is a stochastic process), its signature now has the same properties as a moment-generating function: the powers of Z are replaced by integrals of products of coordinates and Chevyrev & Lyons (2016) show that the expected signature characterizes the law of X.

Moreover, we have the following two properties that make the signature a good feature set in a machine-learning context—precise statements may be found in Bonnier et al. (2019, Appendix A).

Uniqueness Hambly & Lyons (2010) show that under mild assumptions, the full collection of features $\mathrm{Sig}(\mathbf{x}) = \lim_{N \to \infty} \mathrm{Sig}^N(\mathbf{x})$ uniquely determines $\mathbf{x}$ up to translations and reparametrizations.

Universal nonlinearity Linear functionals on the signature are dense in the set of functions on $\mathbf{x}$. Suppose we wish to learn the function f that maps data $\mathbf{x}$ to labels y, the universal nonlinearity property states that, under some assumptions, for any $\varepsilon > 0$, there exists a linear function L such that

$$\|f(\mathbf{x}) - L(\mathrm{Sig}(\mathbf{x}))\| \le \varepsilon. \qquad (1)$$

Note that contrary to Fourier or wavelet basis, signatures provide a natural basis for functions of the time series rather than for the time series itself—equation 1 concerns $f(\mathbf{x})$ and not $\mathbf{x}$. In the context of time series classification this shift of perspective is particularly well-suited since the object of interest is not the time series itself but its link to a label.

From a computational point of view, computing the depth-N signature of a time series $\mathbf{x} \in \mathcal{S}(\mathbb{R}^d)$ of length n has a complexity of $\mathcal{O}(nd^N)$, which can be done with high performance software (Reizenstein & Graham, 2018; Kidger & Lyons, 2020). The size of the depth-N signature

is $(d^{N+1}-1)/(d-1)$ so the memory cost is independent of the series length n, which is a huge advantage when dealing with high frequency time series. Note that small values of N already show a good performance—for example $N = 3$ in the baseline algorithm—so the exponential dependence on N is not a huge computational bottleneck.

Logsignature transform The signature contains some redundant information: for example we can see in the left panel of Figure 1 that the sum of the blue and orange areas is equal to the product of displacements $\Delta X^1 \Delta X^2$:

$$S(\mathbf{x})^{(1,2)} + S(\mathbf{x})^{(2,1)} = S(\mathbf{x})^{(1)} S(\mathbf{x})^{(2)}.$$

The *logsignature transform* is essentially the signature with these redundancies removed. For example, the logsignature encodes the blue and orange areas from the left panel with the orange signed area in the right panel. However, the logsignature does not have a universal nonlinearity property such as equation 1. We refer the reader to Morrill et al. (2020a) or Liao et al. (2019, Section 2) for a precise definition of the logsignature.

A pedagogical introduction to the background theory of signatures is Lyons et al. (2007), whilst a comprehensive textbook is Friz & Victoir (2010). For introductions to the signature method, we recommend Bonnier et al. (2019, Appendix A) and Chevyrev & Kormilitzin (2016).

2.2. Related work

The signature transform has been used in a wide range of applications in machine learning predictive tasks. For example, as mentioned in the introduction, the signature has been used as a feature extraction layer in classifiers for both Arabic (Wilson-Nunn et al., 2018) and Chinese (Yang et al., 2016b) handwriting recognition. Similarly, it was successfully used in human action recognition by Li et al. (2017); Yang et al. (2017); Liao et al. (2019) and in the medical domain as part of the top performing model at the Physionet 2019 challenge for prediction of sepsis (Reyna et al., 2019; Morrill et al., 2019; 2020b). Other applications involve finance (Lyons et al., 2014; Perez Arribas, 2018), mental health (Kormilitzin et al., 2017; Arribas et al., 2018), and emotion recognition (Wang et al., 2019; 2020).

In almost all these applications, the method has been utilised in different ways. Many authors consider transformations of the input time series before application of the signature (Levin et al., 2013; Flint et al., 2016; Lyons & Oberhauser, 2017; Yang et al., 2017; Liao et al., 2019; Kidger & Lyons, 2020; Wu et al., 2020a). People have also explored different windows over which the signature transform should be taken, so as to extract information over different scales (Yang et al., 2017; Bonnier et al., 2019). Additionally a choice must be made between the signature

and logsignature transforms, as must choices for the scaling of the terms in the signature (Chevyrev & Kormilitzin, 2016; Lai et al., 2017).

The differences between some of these choice have been shown by Fermanian (2019) to significantly impact the performance of the methodology. However this study used a small collection of datasets and considered only some of the most common variations that exist in the literature. There is therefore a need for a comprehensive study and unification of all these different choices.

3. The generalized signature method

In this section we collate the modifications to the signature transform that have been proposed in signature literature to date. We will show that each can be categorised into one of the following groups:

- **Augmentations** These describe the transformation of a time series into one or more new series, in order to return different information in the signature features and deal with dimensionality issues.

- **Windows** Splitting the time series over different subsequences (or windows), so that signatures may be applied locally.

- **Transform** The choice between the signature or the logsignature transform.

- **Rescaling** Ways of normalising the terms in the signature.

We then go on to show that these groupings can themselves be synergised into a single mathematical framework that we term *the generalised signature method*. For clarity, we will begin by discussing each of these individually, and then afterwards show how they may be combined.

As before, assume that we observe some collection of sequences $\mathbf{x} \in \mathcal{S}(\mathbb{R}^d)$ with timestamps $\mathbf{t} \in \mathcal{S}(\mathbb{R})$.

3.1. Augmentations

We define an *augmentation* to be a transform of an initial sequence $\mathbf{x} \in \mathcal{S}(\mathbb{R}^d)$ into one or several new sequences. Augmentations have several different uses:

1. Remove the signature invariance to translation and/or reparametrization.

2. Lower the dimension d of the time series, so that higher orders of the signature are reachable—recall that the depth-N signature is of size $\mathcal{O}(d^N)$.

3. Preprocess the time series prior to the signature map so that information is more easily extracted.

For some $e, p \in \mathbb{N}$, we define an augmentation as a map

$$\phi \colon \mathcal{S}(\mathbb{R}^d) \to \mathcal{S}(\mathbb{R}^e)^p.$$

There are many pre-signature operations which have been proposed in the literature, and which we categorise as augmentations. We refer the reader to Appendix A for full details of the many such operations proposed in the literature, but will focus on several important examples here.

Let us give some examples in the first group of sensitivity-inducing augmentations. For any vector of increasing timestamps $\mathbf{t}$, we call *time augmentation* (Levin et al., 2013) the operation $\phi_{\mathbf{t}} : \mathcal{S}(\mathbb{R}^d) \mapsto \mathcal{S}(\mathbb{R}^{d+1})$ defined by

$$\phi_{\mathbf{t}}(\mathbf{x}) = \big((t_1, x_1), \ldots, (t_n, x_n)\big). \tag{2}$$

This transformation, which basically consists in adding the timestamps as an extra coordinate, has two key properties: it guarantees the uniqueness of the signature (Hambly & Lyons, 2010) and it adds information about the parametrization of the time series.

Another example is the basepoint augmentation (Kidger & Lyons, 2020), which is the map $\phi^b : \mathcal{S}(\mathbb{R}^d) \mapsto \mathcal{S}(\mathbb{R}^d)$ defined by

$$\phi^b(\mathbf{x}) = (0, x_1, \ldots, x_n), \tag{3}$$

which simply adds a zero at the beginning of the time series—note that this zero could also be put at the end. This transformation makes the signature sensitive to translations of the time series. The invisibility-reset transformation (Yang et al., 2017; Wu et al., 2020b) also adds translation sensitivity, but does so by increasing the dimension.

In the second group of augmentations for dimensionality reduction, we consider random projections (Lyons & Oberhauser, 2017), which consist in applying multiple random linear maps to the time series, or coordinate projections, which project along (multiple subsets of) the coordinate axes.

In the third group, the lead-lag augmentation (Chevyrev & Kormilitzin, 2016; Flint et al., 2016; Yang et al., 2017) captures the quadratic variation by transforming the time series to

$$\phi(\mathbf{x}) = \big((x_1, x_1), (x_2, x_1), (x_2, x_2), (x_3, x_2), (x_3, x_3),$$
$$\ldots, (x_n, x_n)\big) \in \mathcal{S}(\mathbb{R}^{2d}).$$

Another important example of this kind of augmentation are the stream preserving neural networks of Bonnier et al. (2019), who learn a map ϕ from the data. They map a time series in $\mathbb{R}^d$ to another series in $\mathbb{R}^e$ by setting ϕ to some neural network, typically either convolutional or recurrent. We extend this idea by defining the multi-headed stream preserving augmentation, which simply consists in

stacking p such transformations. To our knowledge, this is the first time that such learned augmentations are compared to 'handcrafted' ones such as time, basepoint and lead-lag augmentations.

Importantly, these various augmentations may be combined together. For example, in order to add sensitivity to both parametrization and translation, the time and basepoint augmentations may be combined: first apply the time augmentation, which gives a sequence $\phi_{\mathbf{t}}(x) \in \mathcal{S}(\mathbb{R}^{d+1})$, and then the basepoint augmentation, which yields

$$\phi^b \circ \phi_{\mathbf{t}}(\mathbf{x}) = \big((0,0),(t_1,x_1),\ldots,(t_n,x_n)\big). \quad (4)$$

3.2. Windows

The second step is to choose a windowing operation. Much like the window functions used with a short time Fourier transform, this localises the signature computation to extract information over particular time intervals.

We define a window to be a map

$$W \colon \mathcal{S}(\mathbb{R}^e) \to \mathcal{S}(\mathbb{R}^e)^w,$$

for some $w \in \mathbb{N}$. In short, W maps a time series in $\mathbb{R}^e$ into w new time series in the same space. The simplest possible window is the global window, defined by

$$W(\mathbf{x}) = (\mathbf{x}), \quad (5)$$

which outputs the time series itself. To get finer-scale information, we consider three other types of windows: sliding, expanding and hierarchical dyadic windows. For $\mathbf{x} = (x_1,\ldots,x_n) \in \mathcal{S}(\mathbb{R}^e)$ and $1 \le i \le j \le n$, let $\mathbf{x}_{i:j} = (x_i,\ldots,x_j) \in \mathcal{S}(\mathbb{R}^e)$ be a subsequence of $\mathbf{x}$. Then, a sliding window of length ℓ and step l is defined by

$$W(\mathbf{x}) = (\mathbf{x}_{1:\ell}, \mathbf{x}_{l+1:l+\ell}, \mathbf{x}_{2l+1:2l+\ell}, \ldots),$$

and an expanding window of initial length ℓ and step l by

$$W(\mathbf{x}) = (\mathbf{x}_{1:\ell}, \mathbf{x}_{1:l+\ell}, \mathbf{x}_{1:2l+\ell}, \ldots).$$

The expanding window produces time series of increasing length, and is analogous to the history processes of stochastic analysis whereas the sliding window produces time series of fixed length but shifted in time.

Finally we consider a hierarchical dyadic window, which captures information at different scales. Let $q \in \mathbb{N}$ be fixed and assume for simplicity that 2^{q-1} divides n. Then, the hierarchical dyadic window of depth q consists of q sliding windows $W^1,\ldots,W^q$, where W^i has length and step both equal to $n2^{-(i-1)}$. This yields $w = 2^q - 1$ time series of length n, $n/2$, $n/4$, $\ldots$, $n/2^{q-1}$. The larger the value of q, the finer the scale on which the information is extracted. If the other window functions are analogous to the short time Fourier transform, then hierarchical dyadic windows are analogous to the multi-scale nature of wavelets.

3.3. The signature and logsignature transforms

Central to the signature methodology is of course the signature transform itself. Two choices must be made; whether to use the signature or logsignature transform, and what depth to calculate the transform to—that is, what depth N in Definition 2 to use. Choosing a logsignature lowers the feature vector dimension at the cost of loosing linear approximation properties. There is no consensus on which one should be favored for a machine learning task.

3.4. Rescaling

The depth-k term in the signature is of size $\mathcal{O}(1/k!)$. Typically, rescaling these terms to $\mathcal{O}(1)$ will aid in subsequent learning procedures. To this end, we can apply *pre-signature* scaling whereby we scale the path before signature computation, or *post-signature* where we scale the signature terms themselves. Specifics on how this is done in practice are given in Appendix B.

3.5. Putting the pieces together

Let $\phi \colon \mathcal{S}(\mathbb{R}^d) \to \mathcal{S}(\mathbb{R}^e)^p$ be the final augmentation function, $\phi : \mathbf{x} \mapsto \big(\phi^1(\mathbf{x}),\ldots,\phi^p(\mathbf{x})\big)$, which can be a composition of augmentations such as equation 4. Let $W : \mathcal{S}(\mathbb{R}^e) \to \mathcal{S}(\mathbb{R}^e)^w$, $W : \mathbf{x} \mapsto \big(W^1(\mathbf{x}),\ldots,W^w(\mathbf{x})\big)$, be the window map, such that $W^j(\mathbf{x}) \in \mathcal{S}(\mathbb{R}^e)$ for any $1 \le j \le w$. Let S^N represent either the signature or logsignature transform of depth N. Let ρ_{pre} and ρ_{post} represent the different types of features rescaling. Then given an input $\mathbf{x} \in \mathcal{S}(\mathbb{R}^d)$, the general framework for extracting signature features is given by the collection of

$$\mathbf{z}_{i,j} = (\rho_{\text{post}} \circ S^N \circ \rho_{\text{pre}} \circ W^j \circ \phi^i)(\mathbf{x}) \quad (6)$$

over all $i \in \{1,\ldots,p\}$, $j \in \{1,\ldots,w\}$. We refer to the procedure of computing $\mathbf{x} \mapsto (\mathbf{z}_{i,j})$ as the *generalised signature method*.

This final procedure is a little involved, but is simply a combination of different elementary operations used to impact the final feature set. The overall procedure now offers a degree of flexibility and generality which has, to our knowledge, never been achieved for signature methods.

The collection of features $(\mathbf{z}_{i,j})$ may then be fed into any later machine learning algorithm, which will depend on the application. In general, the $\mathbf{z}_{i,j}$ will be stacked together and considered as a vector. However, if one wants to use a sequential algorithm such as a recurrent network, it is possible to turn the features $\mathbf{z}_{i,j}$ into a sequence by choosing a sliding or expanding window. Indeed, these windows induce an ordering in the features: the terms $\mathbf{z}_{i,1}$ will correspond to the first values of $\mathbf{x}$, the terms $\mathbf{z}_{i,2}$ to the following values, and so on.

4. Empirical study

We perform a first-of-its-kind empirical study across 26 datasets to determine the most important aspects of this framework.

4.1. Methodology

Datasets The datasets used are the Human Activities and Postural Transitions dataset provided by Reyes-Ortiz et al. (2016), the Speech Commands dataset provided by Warden (2018), and 24 datasets from the UEA time series classification archive, provided by Bagnall et al. (2018). A few datasets from the UEA archive were excluded due to their high number of channels resulting in too large a computational burden.

Baseline We begin by defining a single baseline procedure, representing a simple and straightforward collection of choices for the generalised signature method. This baseline is to take the augmentation ϕ as appending time as defined by equation 2, W as the global window defined by equation 5, have the transform be a signature transform of depth 3, and to use pre-signature scaling of the path. This means that the input features are the collection

$$\mathbf{z} = \mathrm{Sig}^3 \circ \rho_{\mathrm{pre}} \circ \phi_{\mathbf{t}}(\mathbf{x}).$$

Individual variations With respect to this baseline procedure, we then consider, in turn, the groups described in Section 3. These were *augmentations*, *windows*, *transform*, and *rescaling*. For each group we modify the baseline by implementing each option in the group one-by-one. Each such variation defines a particular form of the generalised signature method as in equation 6. Example variations are to switch to using a logsignature transform of depth 5, or to use a sliding window instead of a global window. We discuss the precise variations below.

Models On top of every variation, we then consider four different models: logistic regression, random forest, Gated Recurrent Unit (GRU) (Cho et al., 2014), and a residual Convolutional Neural Network (CNN) (He et al., 2015). We test nearly every combination of dataset, variation of the generalised signature method, and model. Different datasets and variations produce different numbers of features $\mathbf{z}_{i,j}$, so to reduce the computational burden we omit those cases for which the number of features is greater than 10^5. Of the 9984 total combinations of dataset, variation, and model, this leaves out 1415 combinations. See Appendix C.2 for a break down of the omitted combinations by different cases.

Analysis We define the performance of a variation on a dataset as the best performance across the four models considered, to reflect the fact that different models are better suited for different problems. We then follow the methodology of Demšar (2006); Benavoli et al. (2016); Ruiz et al. (2020) to compare the variations across the multiple datasets. We first perform a Friedman test to reject the null hypothesis that all methods are equivalent. If it is rejected, we perform pairwise Wilcoxon signed-rank tests to form cliques of not-significant methods, and use critical difference plots to visualize the performance of each signature method.

A critical difference plot shows the different variations ordered by their average rank: for example, in Figure 2, the best variation is "Time + Basepoint" with an average rank of 2.5. Then, a thick line indicates that the Wilcoxon test between variations inside the clique is not rejected at significance threshold of 5%, subject to Bonferroni's multiple testing correction. In Figure 2 there are two groups of significantly different variations: one with "Basepoint" and "None" and one with all other variations.

We refer the reader to Appendix C for further details on the methodology, such as precise architectural choices, learning rates, and so on.

4.2. Results

Due to the large number of variations and datasets considered, we present only the critical difference plots in the main paper. See Appendix D for all the tables of the underlying numerical values.
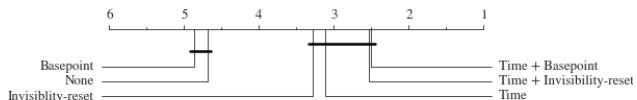
Figure 2. Performance of invariance-removing augmentations.

Augmentations We split the augmentations into two categories. The first category consists of those augmentations which remove the signature's invariance to translation (basepoint augmentation, invisibility-reset augmentation) or reparameterisation (time augmentation). We see in Figure 2 that augmenting with time, and either basepoint or invisibility-reset, are both typically important. This is expected; in general a problem need not be invariant to either translation or reparametersiation.
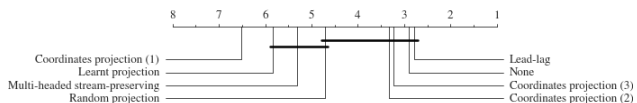
Figure 3. Performance of other augmentations.

The second category consists of those augmentations which either seek to reduce dimensionality or introduce additional information. We see in Figure 3 that most augmentations actually do not help matters, except for lead-lag which usually represents a good choice. We posit that the best augmentation is likely to be dataset dependent, so we break this down by dataset characteristics in Table 6.

Table 1. Average ranks for different augmentations by data type. Lower is better. CP (2) stands for coordinate projections with pairs and LP for Learnt projections.

	Augmentation				
Data type	None	Lead-lag	CP (2)	LP	MHSP
EEG	4.88	4.83	3.13	**2.75**	**2.75**
HAR	2.25	**1.78**	3.50	6.50	6.50
MOTION	2.63	**1.75**	4.50	7.33	5.00
OTHER	2.88	3.92	**2.63**	6.00	5.21

Here we indeed see that there is generally a better choice than doing nothing at all, but that this better choice is dependent on some characteristic of the dataset. For example, learnt projections and multi-headed stream preserving transformations do substantially better on EEG datasets, while lead-lag is better for human action and motion recognition.
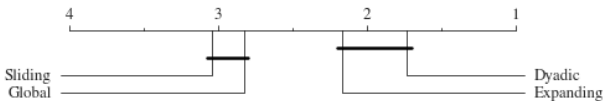
Figure 4. Performance of different windows.

Windows We consider the possibility of global, sliding, expanding, and dyadic windows. The results are shown in Figure 4. We see that the dyadic and expanding windows are significantly better than sliding and global windows. The poor performance of sliding windows is a little surprising, but tallies with the observations of Fermanian (2019). This is an important finding, as global and sliding windows tend to be commonly used with signature methods.

Signature versus logsignature transforms We consider the signature and logsignature transforms with depths ranging from 1 to 6. As higher depths always produce more information, we define the performance of the (log)signature transform as the best performance across all depths. With this metric, the signature transform is significantly better than the logsignature transform, with a p-value of 0.01 for the Wilcoxon signed-rank test.

The key results To conclude, these results show that invariance-removing transformations such as time and basepoint augmentations should a priori be used, that the lead-lag performs well but not significantly better than no additional augmentation, and that the hierarchical dyadic window performs significantly better than the sliding and global ones. The poor performance of deep learning approaches for augmentation is also notable and an additional motivation for this work: although slightly technical, the augmentations tailored to the signature transform are a significant addition in a machine learning pipeline and cannot be easily replaced by neural networks.

4.3. Further results

See Appendix D for further results, in particular on the running times, the different types of rescaling, augmentations broken down by dataset characteristics, an additional study on signature depth, and the precise numerical results for each individual test considered here.

5. The canonical signature pipeline

In this section we define *the canonical signature pipeline*. Using the results from Section 4 we evaluate the top performing options over all the datasets so as to provide a domain-agnostic starting point for any dataset, from which other variations can be easily explored. We show that this pipeline shows competitive performance against traditional benchmarks and even against deep neural networks.

5.1. Definition

In a nutshell, the pipeline consists in applying the basepoint and time augmentations, a hierarchical dyadic window and a signature transform, which can be written as a particular case of equation 6 as follows. Let W be a hierarchical dyadic window of depth q, $\phi_{\mathbf{t}}$ and ϕ^b be the time and basepoint augmentations, then the canonical signature pipeline may be written as

$$\mathbf{z}_j = S^N \circ W^j \circ \phi^b \circ \phi_{\mathbf{t}}(\mathbf{x}), \quad j \in \{1, \ldots, 2^q - 1\}. \quad (7)$$

We give a graphical depiction of this in Figure 5. Signature and window depths (N, q) must be optimised for the problem (typically via cross-validation). We note that this canonical method may be adapted to the problem at hand in two ways: if the problem is known to be parametrization invariant, as is the case for example for characters recognition, then the time augmentation should not be applied. Moreover, if the problem is translation-invariant, then the basepoint augmentation is not applied. We emphasise that this pipeline does not represent a best option for every application, but is meant to represent a compromise between broad applicability, ease of implementation, computational cost, and good performance.
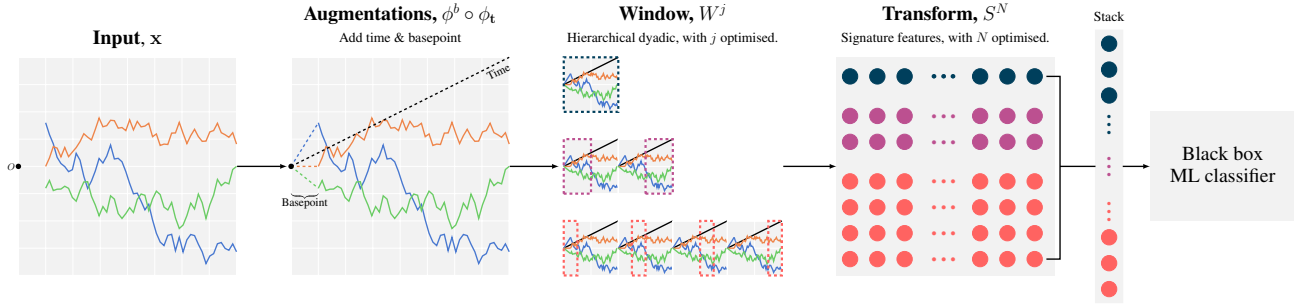
Figure 5. Pictorial representation of the canonical signature pipeline. First, we apply the time and basepoint augmentations to the input paths, then we compute the signature features over dyadic windows, and finally compute the signature features over each dyadic window. These features can now be compiled together and fed into any standard machine learning classifier.

5.2. Performance

We validate the performance of the pipeline against the 26 datasets in the multivariate UEA archive[1]. To our knowledge, the most recent benchmarks for the UEA archive are the results from Ruiz et al. (2020). We compare their results to the canonical signature pipeline with a random forest classifier—see Appendix C.3 for more details.

The benchmarks include variants on classical Dynamic Time Wrapping (DTWI, DTWD and DTWA); an ensemble of univariate classifiers, HIVE COTE (Bagnall et al., 2020), known to be highly perfromant in the univariate case; a random shapelet forest (Karlsson et al., 2016), denoted gRSF, and a bag of words based algorithm, MUSE (Schäfer & Leser, 2017); two deep learning methods, TapNet (Wang et al., 2017) and MLCN (Karim et al., 2019). The MLCN architecture combines long short term memory layers (LSTM) and convolutional layers while TapNet combines 3 blocks: random projections on the different dimensions, convolutional layers and a final attention block to compare candidate time series representations.
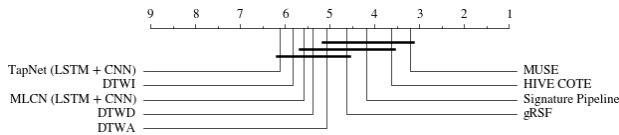
Figure 6. Performance on UEA datasets.

Figure 6 shows the critical difference plot of this comparison. The signature pipeline is in the first clique, that is the group of classifiers that achieve the best accuracy while not being significantly different from one another. The two algorithms with a better rank than the signature

pipeline are MUSE and HIVE-COTE. It is worth noting that MUSE is very memory intensive—Ruiz et al. (2020) report that it could not finish on 5 of the 26 UEA datasets on a computer with 500GB of memory—whilst HIVE-COTE is an ensemble of several sub-classifiers, and thus has very high training and inference costs. On the other hand, all experiments for the canonical signature pipeline were completed with no memory errors on a computer with less memory, and are significantly faster to run than HIVE-COTE—see Appendix D.

The canonical signature pipeline is meant to be a sensible starting point from which the user can propose additional variations following the structure defined in equation 6, but as a standalone classifier this pipeline performs comparably to state-of-the-art classifiers, on the UEA data, whilst being less computationally demanding.

6. Conclusion

We introduce a generalised signature method as a framework to capture recently proposed variations on the signature method. We go on to perform a first-of-its-kind extensive empirical investigation as to which elements of this framework are most important for performance in a domain-independent setting. In particular, we highlight the performance of hierarchical dyadic windows and signature-tailored augmentations such as lead-lag, time and basepoint. As a result, we are able to present a canonical signature pipeline that represents a best-practices domain-agnostic starting point, which shows competitive performance against state-of-the-art classifiers for multivariate time series classification.

References

Arribas, I. P., Goodwin, G. M., Geddes, J. R., Lyons, T., and Saunders, K. E. A signature-based machine learning model for distinguishing bipolar disorder and borderline personality disorder. *Translational psychiatry*, 8:1–7,

---

[1]This is not to be confused with the UCR archive which is a collection of 128 univariate datasets.

2018.

Bagnall, A., Dau, H. A., Lines, J., Flynn, M., Large, J., Bostrom, A., Southam, P., and Keogh, E. The uea multivariate time series classification archive, 2018. *arXiv:1811.00075*, 2018.

Bagnall, A. J., Flynn, M., Large, J., Lines, J., and Middlehurst, M. A tale of two toolkits, report the third: on the usage and performance of hive-cote v1. 0. *CoRR*, 2020.

Benavoli, A., Corani, G., and Mangili, F. Should we really use post-hoc tests based on mean-ranks? *The Journal of Machine Learning Research*, 17:152–161, 2016.

Bonnier, P., Kidger, P., Perez Arribas, I., Salvi, C., and Lyons, T. Deep Signature Transforms. In *Advances in Neural Information Processing Systems*, pp. 3099–3109, 2019.

Chevyrev, I. and Kormilitzin, A. A primer on the signature method in machine learning. *arXiv:1603.03788*, 2016.

Chevyrev, I. and Lyons, T. Characteristic functions of measures on geometric rough paths. *The Annals of Probability*, 44(6):4049–4082, 2016.

Cho, K., van Merrienboer, B., Gulcehre, C., Bougares, F., Schwenk, H., and Bengio, Y. Learning Phrase Representations using RNN Encoder-Decoder for Statistical Machine Translation. *EMNLP 2014*, 2014.

Demšar, J. Statistical comparisons of classifiers over multiple data sets. *Journal of Machine learning research*, 7:1–30, 2006.

Fermanian, A. Embedding and learning with signatures. *arXiv:1911.13211*, 2019.

Flint, G., Hambly, B., and Lyons, T. Discretely sampled signals and the rough Hoff process. *Stochastic Processes and their Applications*, 126:2593–2614, 2016.

Friz, P. K. and Victoir, N. B. *Multidimensional Stochastic Processes as Rough Paths: Theory and Applications*, volume 120 of *Cambridge Studies in Advanced Mathematics*. Cambridge University Press, Cambridge, 2010.

Futoma, J., Hariharan, S., and Heller, K. Learning to detect sepsis with a multitask Gaussian process RNN classifier. In *Proceedings of the 34th International Conference on Machine Learning*, pp. 1174–1182, 2017.

Grabocka, J., Schilling, N., Wistuba, M., and Schmidt-Thieme, L. Learning time-series shapelets. In *Proceedings of the 20th ACM SIGKDD international conference on Knowledge discovery and data mining*, pp. 392–401, 2014.

Greff, K., Klein, A., Chovanec, M., Hutter, F., and Schmidhuber, J. The sacred infrastructure for computational research. In *Proceedings of the Python in Science Conferences-SciPy Conferences*, 2017.

Hambly, B. M. and Lyons, T. J. Uniqueness for the signature of a path of bounded variation and the reduced path group. *Annals of Mathematics*, 171:109–167, 2010.

He, K., Zhang, X., Ren, S., and Sun, J. Deep Residual Learning for Image Recognition. *arXiv:1512.03385*, 2015.

Karim, F., Majumdar, S., Darabi, H., and Harford, S. Multivariate lstm-fcns for time series classification. *Neural Networks*, 116:237–245, 2019.

Karlsson, I., Papapetrou, P., and Boström, H. Generalized random shapelet forests. *Data mining and knowledge discovery*, 30(5):1053–1085, 2016.

Kidger, P. and Lyons, T. Signatory: differentiable computations of the signature and logsignature transforms, on both CPU and GPU. *arXiv:2001.00706*, 2020. URL https://github.com/patrick-kidger/signatory.

Kidger, P., Morrill, J., and Lyons, T. Generalised Interpretable Shapelets for Irregular Time Series. *arXiv:2005.13948*, 2020.

Kingma, D. P. and Ba, J. Adam: A method for stochastic optimization. In *Proceedings of International Conference on Learning Representations*, 2015.

Kormilitzin, A., Saunders, K., Harrison, P., Geddes, J., and Lyons, T. Application of the signature method to pattern recognition in the cequel clinical trial. *arXiv:1606.02074*, 2016.

Kormilitzin, A., Saunders, K. E., Harrison, P. J., Geddes, J. R., and Lyons, T. Detecting early signs of depressive and manic episodes in patients with bipolar disorder using the signature-based model. *arXiv preprint arXiv:1708.01206*, 2017.

Lai, S., Jin, L., and Yang, W. Online signature verification using recurrent neural network and length-normalized path signature descriptor. In *Proceedings of the 14th IAPR International Conference on Document Analysis and Recognition (ICDAR)*, volume 1, pp. 400–405. IEEE, 2017.

Levin, D., Lyons, T., and Ni, H. Learning from the past, predicting the statistics for the future, learning an evolving system. *arXiv:1309.0260*, 2013.

Li, C., Zhang, X., and Jin, L. LPSNet: a novel log path signature feature based hand gesture recognition framework. In *Proceedings of the IEEE International Conference on Computer Vision*, pp. 631–639, 2017.

Li, S. C.-X. and Marlin, B. M. A scalable end-to-end Gaussian process adapter for irregularly sampled time series classification. In *Advances in Neural Information Processing Systems*, pp. 1804–1812, 2016.

Liao, S., Lyons, T., Yang, W., and Ni, H. Learning stochastic differential equations using RNN with log signature features. *arXiv:1908.08286*, 2019.

Lyons, T. and Oberhauser, H. Sketching the order of events. *arXiv:1708.09708*, 2017.

Lyons, T., Ni, H., and Oberhauser, H. A feature set for streams and an application to high-frequency financial tick data. In *Proceedings of the 2014 International Conference on Big Data Science and Computing*, pp. 5. ACM, 2014.

Lyons, T. J., Caruana, M., and Lévy, T. *Differential Equations driven by Rough Paths*, volume 1908 of *Lecture Notes in Mathematics*. Springer, Berlin, 2007.

Moor, M., Horn, M., Bock, C., Borgwardt, K., and Rieck, B. Path Imputation Strategies for Signature Models. *arXiv:2005.12359*, 2020.

Morrill, J., Kormilitzin, A., Nevado-Holgado, A., Swaminathan, S., Howison, S., and Lyons, T. The signature-based model for early detection of sepsis from electronic health records in the intensive care unit. *International Conference in Computing in Cardiology*, 2019.

Morrill, J., Kidger, P., Salvi, C., Foster, J., and Lyons, T. Neural CDEs for Long Time-Series via the Log-ODE Method. *arXiv:2009.08295*, 2020a.

Morrill, J. H., Kormilitzin, A., Nevado-Holgado, A. J., Swaminathan, S., Howison, S. D., and Lyons, T. J. Utilization of the signature method to identify the early onset of sepsis from multivariate physiological time series in critical care monitoring. *Critical Care Medicine*, 48(10):e976–e981, 2020b.

Paszke, A., Gross, S., Chintala, S., Chanan, G., Yang, E., DeVito, Z., Lin, Z., Desmaison, A., Antiga, L., and Lerer, A. Automatic differentiation in PyTorch. 2017.

Pedregosa, F., Varoquaux, G., Gramfort, A., Michel, V., Thirion, B., Grisel, O., Blondel, M., Prettenhofer, P., Weiss, R., Dubourg, V., Vanderplas, J., Passos, A., Cournapeau, D., Brucher, M., Perrot, M., and Duchesnay, E. Scikit-learn: Machine learning in Python. *Journal of Machine Learning Research*, 12:2825–2830, 2011.

Perez Arribas, I. Derivatives pricing using signature payoffs. *arXiv*, pp. arXiv–1809, 2018.

Reizenstein, J. and Graham, B. The iisignature library: efficient calculation of iterated-integral signatures and log signatures. *arXiv:1802.08252*, 2018.

Reyes-Ortiz, J.-L., Oneto, L., Samà, A., Parra, X., and Anguita, D. Transition-aware human activity recognition using smartphones. *Neurocomputing*, 171:754–767, 2016.

Reyna, M. A., Josef, C., Seyedi, S., Jeter, R., Shashikumar, S. P., Westover, M. B., Sharma, A., Nemati, S., and Clifford, G. D. Early prediction of sepsis from clinical data: the physionet/computing in cardiology challenge 2019. In *2019 Computing in Cardiology (CinC)*, pp. Page–1. IEEE, 2019.

Ruiz, A. P., Flynn, M., and Bagnall, A. Benchmarking multivariate time series classification algorithms. *arXiv preprint arXiv:2007.13156*, 2020.

Schäfer, P. and Leser, U. Fast and accurate time series classification with weasel. In *Proceedings of the 2017 ACM on Conference on Information and Knowledge Management*, pp. 637–646, 2017.

Tange, O. Gnu parallel - the command-line power tool. *The USENIX Magazine*, 36:42–47, 2011.

Wang, B., Liakata, M., Ni, H., Lyons, T., Nevado-Holgado, A. J., and Saunders, K. A path signature approach for speech emotion recognition. In *Interspeech 2019*, pp. 1661–1665. ISCA, 2019.

Wang, B., Wu, Y., Taylor, N., Lyons, T., Liakata, M., Nevado-Holgado, A. J., and Saunders, K. E. Learning to detect bipolar disorder and borderline personality disorder with language and speech in non-clinical interviews. *arXiv preprint arXiv:2008.03408*, 2020.

Wang, Z., Yan, W., and Oates, T. Time series classification from scratch with deep neural networks: A strong baseline. In *2017 International joint conference on neural networks (IJCNN)*, pp. 1578–1585. IEEE, 2017.

Warden, P. Speech commands: A dataset for limited-vocabulary speech recognition. *arXiv:1804.03209*, 2018.

Wilson-Nunn, D., Lyons, T., Papavasiliou, A., and Ni, H. A path signature approach to online arabic handwriting recognition. In *2018 IEEE 2nd International Workshop on Arabic and Derived Script Analysis and Recognition (ASAR)*, pp. 135–139. IEEE, 2018.

Wu, Y., Ni, H., Lyons, T., and Hudson, R. Signature features with the visibility transformation. *arXiv:2004.04006*, 2020a.

Wu, Y., Ni, H., Lyons, T. J., and Hudson, R. L. Signature features with the visibility transformation. *arXiv preprint arXiv:2004.04006*, 2020b.

Yang, W., Jin, L., and Liu, M. Deepwriterid: An end-to-end online text-independent writer identification system. *IEEE Intelligent Systems*, 31:45–53, 2016a.

Yang, W., Jin, L., Tao, D., Xie, Z., and Feng, Z. Dropsample: A new training method to enhance deep convolutional neural networks for large-scale unconstrained handwritten chinese character recognition. *Pattern Recognition*, 58:190–203, 2016b.

Yang, W., Lyons, T., Ni, H., Schmid, C., Jin, L., and Chang, J. Developing the path signature methodology and its application to landmark-based human action recognition. *arXiv:1707.03993*, 2017.

Ye, L. and Keogh, E. Time series shapelets: a new primitive for data mining. In *Proceedings of the 15th ACM SIGKDD international conference on Knowledge discovery and data mining*, pp. 947–956, 2009.

Supplementary material

A. Augmentations

We recall that an augmentation is a map

$$\phi\colon \mathcal{S}(\mathbb{R}^d) \to \mathcal{S}(\mathbb{R}^e)^p$$

We give below the precise definition of the different augmentations considered in the study, which are summarized in Table 2. These augmentations were not typically introduced using such language, so this serves as a reference for how the existing literature may be interpreted through the generalised signature method.

Throughout the section, we consider a sequence $\mathbf{x} = (x_1, \ldots, x_n) \in \mathcal{S}(\mathbb{R}^d)$ and timestamps $\mathbf{t} = (t_1, \ldots, t_n) \in \mathcal{S}(\mathbb{R})$. We recall that if $\mathbf{x}$ is regularly sampled then $\mathbf{t}$ is usually set to $\mathbf{t} = (1, \ldots, n)$.

Time augmentation We recall the definition of the time augmentation:

$$\phi(\mathbf{x}) = \big((t_1, x_1), \ldots, (t_n, x_n)\big) \in \mathcal{S}(\mathbb{R}^{d+1}).$$

It ensures uniqueness of the signature transformation and removes the parametrization invariance (Levin et al., 2013).

Invisibility-reset augmentation First introduced by Yang et al. (2017), the invisibility-reset augmentation consists in adding a coordinate to the sequence $\mathbf{x}$ that is constant equal to 1 but drops to 0 at the last time step, i.e.,

$$\phi(\mathbf{x}) = \big((1, x_1), \ldots, (1, x_{n-1}), (1, x_n), (0, x_n), (0, 0)\big) \in \mathcal{S}(\mathbb{R}^{d+1}).$$

This augmentation adds information on the initial position of the path, which is otherwise not included in the signature as it is a translation-invariant map.

Basepoint augmentation Introduced by Kidger & Lyons (2020), the basepoint augmentation has the same goal as the invisibility-reset augmentation: removing the translation-invariant property of the signature. It simply adds the point 0 at the beginning of the sequence:

$$\phi(\mathbf{x}) = (0, x_1, \ldots, x_n) \in \mathcal{S}(\mathbb{R}^d).$$

The main difference compared to the invisibility-reset augmentation is that the signature of $\mathbf{x}$ is contained in the signature of the invisibility-reset augmented path, whereas it is not in the signature of the basepoint augmented path. The price paid is that the invisibility-reset augmentation introduces redundancy into the signature, and is more computationally expensive due to the additional channel. (Recall that the signature method scales as $\mathcal{O}(d^N)$, where d is the input channels and N is the depth of the (log)signature.)

Lead-lag augmentation The lead-lag augmentation, introduced by Chevyrev & Kormilitzin (2016) and Flint et al. (2016) has been used in several applications (see for example Lyons et al. (2014); Kormilitzin et al. (2016); Yang et al. (2017)). It adds lagged copies of the path as new coordinates. This then explicitly captures the quadratic variation of the underlying process (Flint et al., 2016). As many different lags as desired may be added. If there is a single lag of a single timestep, then this corresponds to

$$\phi(\mathbf{x}) = ((x_1, x_1), (x_2, x_1), (x_2, x_2), \ldots, (x_n, x_n)) \in \mathcal{S}(\mathbb{R}^{2d}).$$

Coordinate projections For multidimensional streams, one may want to compute the signature of a subset of coordinates individually, rather than the signature of the whole stream; doing so restricts the interaction considered by the signature to just those between the projected coordinates. Let $\mathbf{x^1}, \ldots, \mathbf{x^d} \in \mathcal{S}(\mathbb{R})$ denote the different coordinates of $\mathbf{x} \in \mathcal{S}(\mathbb{R}^d)$.

Then we define the singleton coordinate projection as

$$\phi(\mathbf{x}) = \big((\mathbf{t}, \mathbf{x^1}), (\mathbf{t}, \mathbf{x^2}), \ldots, (\mathbf{t}, \mathbf{x^d})\big) \in \mathcal{S}(\mathbb{R}^2)^d,$$

whilst considering all possible pairs of coordinates yields the augmentation

$$\phi(\mathbf{x}) = \big((\mathbf{t}, \mathbf{x^1}, \mathbf{x^2}), (\mathbf{t}, \mathbf{x^1}, \mathbf{x^3}), \ldots, (\mathbf{t}, \mathbf{x^d}, \mathbf{x^{d-1}})\big) \in \mathcal{S}(\mathbb{R}^3)^{d(d-1)},$$

Table 2. Summary of the different augmentations

	e	p	Property
Fixed augmentations			
None	d	1	
Time	$d+1$	1	sensitivity to parametrization, uniqueness of the signature map
Invisibility-reset	$d+1$	1	sensitivity to translation
Basepoint	d	1	sensitivity to translation
Lead-lag	$2d$	1	information about quadratic variation, uniqueness of the signature map
Coordinates projection			dimensionality reduction
with singletons	2	d	
with pairs	3	$d(d-1)$	
with triplets	4	$d(d^2-1)$	
Random projections	e	p	dimensionality reduction
Learnt augmentations			
Learnt projections	e	p	data-dependent and linear
Stream-preserving neural network	e	1	data-dependent
Multi-headed stream-preserving NN	e	p	data-dependent

and all possible triples yields the augmentation

$$\phi(\mathbf{x}) = \big((\mathbf{t}, \mathbf{x^1}, \mathbf{x^1}, \mathbf{x^2}), (\mathbf{t}, \mathbf{x^1}, \mathbf{x^1}, \mathbf{x^3}), \ldots, (\mathbf{t}, \mathbf{x^d}, \mathbf{x^d}, \mathbf{x^{d-1}})\big) \in \mathcal{S}(\mathbb{R}^4)^{d(d^2-1)}.$$

The decision to always include a time dimension is a somewhat arbitrary one, and it may alternatively be excluded if desired. (This is done so as to make sense of singleton coordinate projections; otherwise the result is a collection of univariate time series, for which the signature extracts only the increment due to the tree-like equivalence property.)

Random projections   When the dimension of the input path is very large, Lyons & Oberhauser (2017) have proposed to project it into a smaller space by taking multiple random projections. Let $e < d$ and let $A_i : \mathbb{R}^d \to \mathbb{R}^e$ be random affine transformations indexed by $i \in \{1, \ldots, p\}$. Then ϕ is defined as

$$\phi(\mathbf{x}) = ((A_1 x_1, \ldots, A_1 x_n), \ldots, (A_p x_1, \ldots, A_p x_n)) \in \mathcal{S}(\mathbb{R}^e)^p.$$

Learnt projections   Rather than taking random projections, Liao et al. (2019) learn it from the data. This takes exactly the same form as the random projections, except that the A_i are learnt.

Stream-preserving neural network   Bonnier et al. (2019) introduce arbitrary learnt sequence-to-sequences maps prior to the signature transform, and refer to such maps, when parameterised as neural networks, as stream-preserving neural networks. For example these may be standard convolutional or recurrent architectures. In general this may be any learnt transformation

$$\phi \colon \mathcal{S}(\mathbb{R}^d) \to \mathcal{S}(\mathbb{R}^e).$$

Multi-headed stream-preserving neural network   A straightforward extension of stream-preserving neural networks is to use multiple such networks, so as to avoid a potential bottleneck through the single signature map that it is eventually used in. Letting $\phi^1, \ldots, \phi^p$ be p different stream-preserving neural networks, then this gives an augmentation

$$\phi(\mathbf{x}) = (\phi^1(\mathbf{x}), \ldots, \phi^p(\mathbf{x})) \in (\mathcal{S}(\mathbb{R}^e))^p.$$

B. Rescaling

The signature transform can be written as a sequence of tensors, indexed by $k \in \{1, \ldots, N\}$. The k-th term is of size $\mathcal{O}(1/k!)$, as it is computed by an integral over a k-dimensional simplex. It is typical that rescaling these terms to be $\mathcal{O}(1)$

will aid subsequent learning procedures.

One option is to simply multiply the k-th term by $k!$, which we call *post-signature* scaling.

However, it is possible that the previous option may suffer from numerical stability issues. Thus we also explore the performance of an option, called *pre-signature scaling*, which may alleviate this, which is to multiply the input $\mathbf{x}$ by some scaling factor $\alpha \in \mathbb{R}$. Then the k-th term will be of size $\mathcal{O}(\alpha^k/k!)$, and so by taking $\alpha = (N!)^{1/N}$ the N-th term in the signature will be $\mathcal{O}(1)$; the trade-off is that Stirling's approximation then shows that the $N/2$-th term will be of size $\mathcal{O}(2^{N/2})$.

C. Implementation details

C.1. General notes

Code All the code for this project is available at [redacted for anonymity].

Libraries The machine learning framework used was PyTorch (Paszke et al., 2017) version 1.3.1. Signatures and logsignatures were computed using the Signatory library (Kidger & Lyons, 2020) version 1.1.6. Scikit-learn (Pedregosa et al., 2011) version 0.22.1 was used for the logistic regression and random forest models. The experiments were tracked using the Sacred framework (Greff et al., 2017) version 0.8.1.

Normalisation Every dataset was normalised so that each channel has mean zero and unit variance.

Architectures Two different GRU models were used on every dataset; a 'small' one with 32 hidden channels and 2 layers, and a 'large' one with 256 hidden channels and 3 layers.

Likewise, two different Residual CNN models were considered. The 'small' one used 6 blocks, each composed of batch normalisation, ReLU activation, convolution with 32 filters and kernel size 4, batch normalisation, ReLU activation, and a final convolution with 32 filters and kernel size 4, so that there are also 32 channels along the 'residual path'. A final two-hidden-layer neural network with 256 neurons was placed on the output. The 'large' is similar, except that it used 128 filters in both the blocks and the residual path, had 8 blocks, used a kernel size of 8, and the final neural network had 1024 neurons.

The logistic regression was performed three times with different amounts of L^2 regularisation, with scaling hyperparameters of 0.01, 0.2 and 1; for every experiment the regularization hyperparameter achieving the best accuracy on the test set was used.

The random forest used the default Scikit-learn implementation with a maximum depth of 6 and 100 trees.

Optimiser The GRU and CNN were optimised using Adam (Kingma & Ba, 2015). The learning rate was 0.01 for the GRU, and 0.001 for the residual CNN. The small models were trained for a maximum of 500 epochs; the large models were trained for a maximum of 1000 epochs. The learning rate was decreased by a factor of 10 if validation loss did not improve over a plateau of 10 epochs. Early stopping was used if the validation loss did not improve for 30 epochs. After training the parameters were always rolled back to those that demonstrated the best validation loss over the course of training. The batch size used varied by dataset; in each it was taken to be the power of two that meant that the number of batches per epoch was closest to 40.

Computing infrastructure Experiments were run on an Amazon AWS G3 Instance (g3.16xlarge) equipped with 4 Tesla M60s, parallelized using GNUParallel (Tange, 2011).

C.2. Analysis of variations of the signature method

Splits The UEA archive comes with a pre-defined train-test split, which we respect. We take an 80%/20% train/validation split in the training data, stratified by class label. For the Human Activities and Postural Transitions dataset, we take a 60%/15%/25% train/validation/test split from the whole dataset. For the Speech Commands dataset, we take a 68%/17%/15% train/validation/test split from the whole dataset. (These somewhat odd choices corresponding to taking either 25% or 15% of the dataset as test, and then splitting the remaining 80%/20% between train and validation.) These

train/validation splits are only used for the training of the GRU and CNN classifiers.

Combinations In total we tested 8569 different combinations.

The variations tested are divided into groups. The first group consists of the sensitivity-adding augmentations, namely time, basepoint and invisibility-reset. Relative to the baseline model, we test every possible combination of these. (Including using none of them.)

The second group consists of those other augmentations, namely the lead-lag, singleton coordinate projection, pair coordinate projection, triplet coordinate projection, random projections, learnt projections, and multi-headed stream preserving neural networks, and finally also the case of no additional augmentation.

For the random projections, we consider four possibilities, with $e \in \{3, 6\}$ and $p \in \{2, 5\}$, all relative to the baseline model.

For no additional augmentation, lead-lag, coordinate projections, learnt projections, and the multi-headed stream preserving neural networks, we compose them with the time, time+basepoint and time+invisibility-reset augmentations (the clear best three from the first group), all relative to the baseline model.

For the learnt projections, we consider four different possibilities corresponding to $e \in \{3, 6\}$ and $p \in \{2, 5\}$; together with the time/time+basepoint/time+invisibility-reset cases this yields a total of twelve possibilities.

For the multi-headed stream-preserving neural networks, we again consider four different possibilities corresponding to $e \in \{3, 6\}$ and $p \in \{2, 5\}$, for a total of twelve possible augmentation strategies. In each the neural network operates elementwise, so as to map one sequence to another, and is given by a feedforward neural network of three hidden layers separated by ReLU activation functions. When $e = 3$ the hidden layers have 16 neurons each, and when $e = 6$ they have 32 neurons each.

For both the learnt projections and multi-headed stream-preserving neural networks, training these requires backpropagating through the model, so these were only considered for the GRU and residual CNN model. (The logistic regression model would in principle be possible as well, except that we ended up implementing this through Scikit-learn rather than PyTorch.)

We note that there are a great many possible ways of doing stream preserving neural networks, of which these are a small fraction. Their relatively weak performance here may likely be improved upon with greater tuning on an individual task, or the selection of better final models than were considered here.

The third group consisted of the different windows. Recall that the baseline model used a global window; we then consider varying this to two possible sliding windows, two possible expanding windows, and three possible dyadic windows. The two possible sliding/expanding windows are chosen so that either 5 or 20 windows are applied across the full length of the dataset. The three possible dyadic windows are depths 2, 3, 4. Thus in total there are 8 possible window combinations we consider.

The fourth group consists of rescaling options, namely no rescaling, pre-signature rescaling, and post-signature rescaling.

Omissions For the empirical study on the variations on the signature method, we excluded those UEA datasets with a dimension d over 60, so as to reduce the computational cost. This results removes 6 of the 30 datasets from the study, namely DuckDuckGeese, FaceDetection, Heartbeat, InsectWingbeat, MotorImagery, and PEMS-SF. These were nonetheless used in the demonstration of performance of the canonical signature method in Figure 6. Furthermore those combinations of dataset/variation/model which produced more than 10^5 signature features were omitted, to keep the computation managable. See Table 3.

C.3. The canonical signature pipeline

For each dataset, we implement the following steps. First, the sequences are augmented with time and basepoint augmentations. Then, we consider every combination of signature depth in $\{1, 2, 3, 4, 5, 6\}$ and hierarchical dyadic window depth in $\{2, 3, 4\}$. For each of these choices, we perform a randomized grid search on a random forest classifier to optimize

Table 3. Summary of the number of combinations considered and omitted.

Variations	# Variations	# Classifiers	# Omitted Combinations	# Total Combinations
Basic augmentations (Figure 2)	6	6	54	936
Other augmentations (Figure 3)				
Lead-lag/ None	3	6	100/27	468
Coordinates projection (1)/(2)/(3)	3	6	12/12/54	468
Random projections	4	6	32	624
Learnt projections / MHSP	12	4	348/176	1248
Windows (Figure 4)	8	6	227	1248
Signature/Logsignature transform	12	6	361	1872
Rescalings (Figure 8)	3	6	12	468
Total			1415	9984

its number of trees and maximal depth parameters. We test 20 combinations randomly sampled from the following grids:

$$\text{n\_trees} = [50, 100, 500, 1000],$$
$$\text{max\_depth} = [2, 4, 6, 8, 12, 16, 24, 32, 45, 60, 80, \text{None}].$$

Note that a maximal depth set to 'None' means that the trees are expanded until all leaves contain exactly one sample. Finally, we choose the combination of signature and hierarchical dyadic window depths which maximise the out-of-bag score.

D. Additional results

D.1. Analysis of variations of the signature method

Running time   To get a sense of the cost of each augmentation or window, we present the run times of each augmentation/model combination, and each window/model combination. (The times for varying between signature and logsignature, and between different rescalings, are largely insignificant.) See Table 4.

The run times are averaged over every UEA dataset. As the datasets are of very different sizes this thus represents quite a crude statistic, and in particular produces very large variances, so these are most meaningful simply with respect to each other.

Sensitivity-inducing augmentations broken down by dataset type   Table 5 shows the average rank of each of the first group of augmentations (that add sensitivity to certain kinds of perturbation) by dataset type, where the types are taken from Bagnall et al. (2018). (This may be regarded as a companion to Table 6.)

It is interesting to note that for EEG data, it seems better not to consider the time augmentation, whereas it is the case for other applications. In particular the combination of time and basepoint augmentations achieve the best ranks for human action and motion recognition (HAR and MOTION in Table 5). Recognizing an action may not be translation-invariant nor invariant by time reparametrization.

Other augmentations broken down by dataset characteristichs   Table 6 presents the average ranks of the other augmentations borken down by some characteristics of the datasets.

Here we see that there is generally a better choice than doing nothing at all, but that this better choice. For example on long or high-dimensional datasets, coordinate projections often perform well, whilst multi-headed stream preserving transformations do substantially better on EEG datasets. Lead-lag remains a strong choice in many cases.

Depth study on the signature transform   In the main text we focused on the difference between the signature and logsignature transforms, and stated that larger depths must be chosen by a bias-variance tradeoff. Here we consider varying

Table 4. Average run time (in seconds) for various experiments. mean (std), averaged over all UEA datasets.

	Classifier			
	CNN	GRU	Logistic regression	Random forest
Time augment & Global window (Baseline)	69.8 (98.0)	22.2 (31.8)	2.67 (7.09)	2.23 (4.84)
Augmentation				
None	48.1 (63.5)	16.8 (33.6)	3.55 (9.91)	66.3 (321)
Lead-lag	48.58 (69.99)	15.2 (18.1)	5.76 (11.7)	3.35 (6.04)
Coordinates projection (1)	32.8 (31.49)	13.4 (17.8)	1.37 (4.2)	12.2 (59.3)
Coordinates projection (2)	41.5 (51.4)	22.6 (62.3)	3.01 (8.54)	42.3 (203)
Coordinates projection (3)	41.3 (39.9)	19.1 (24.5)	5.41 (9.76)	6.3 (14.1)
Random projection	62.2 (70.1)	21.1 (31.2)	0.86 (1.25)	1.4 (2.47)
Learnt projection	917 (1288)	752 (972)	–	–
Multi-headed stream-preserving	1051 (1677)	1758 (4442)	–	–
Window				
Sliding	90.6 (120)	79.4 (175)	10.1 (27.4)	6.4 (16.0)
Expanding	102 (133)	68.7 (115)	9.98 (27.2)	7.17 (19.0)
Dyadic	725 (868)	56.9 (65.1)	12.5 (33.2)	7.59 (18.3)

Table 5. Average ranks for different augmentations by type of data. Lower is better.

	Augmentation					
Data type	None	Time	Basepoint	Invisibility-reset	Time + Basepoint	Time + Invisibility-reset
EEG	3.88	3.50	4.00	**2.00**	4.00	3.63
HAR	5.00	2.95	4.85	3.65	**2.00**	2.55
MOTION	5.25	2.75	5.75	3.88	**1.50**	1.88
OTHER	4.43	3.31	4.88	3.19	2.87	**2.31**

the depth together with the choice of signature or logsignature, and taking the best transform for each depth. See Figure 7. We see that larger depths do indeed generally correspond to increased performance, up to a point. The optimal depth will depend on the complexity of the task, as the number of features increases exponentially with the depth.
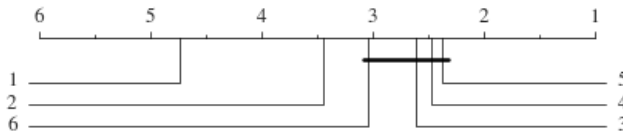
Figure 7. Critical differences plot for the depth study on the UEA datasets.

Rescaling critical difference diagram In Figure 8, we see that pre-signature rescaling performs significantly worse than the other two options and that no significant difference between post-rescaling and no rescaling is found.

D.2. Complete results

We present in Tables 7, 8, 9, 10, 11 and 12 the performance of the different signature variations on each dataset. The tables were obtained by maximizing the test accuracy of the signature method over the different classifiers considered. Recall that some values are omitted due to the large number of signature features that would be obtained.

Table 6. Average ranks for different augmentations by dataset characteristics. Lower is better.

Characteristic	None	Lead-lag	Coordinates projection			Random Projection	Learnt Projection	MHSP
			(1)	(2)	(3)			
Data type								
EEG	4.88	4.83	6.50	3.13	5.67	4.38	**2.75**	**2.75**
HAR	2.25	**1.78**	7.20	3.50	2.90	4.75	6.50	6.50
MOTION	2.63	**1.75**	7.00	4.50	2.13	5.00	7.33	5.00
OTHER	2.88	3.92	5.44	**2.63**	3.29	4.69	6.00	5.21
Series length								
<50	3.20	**2.20**	7.40	3.20	2.70	5.10	7.00	5.20
50-100	2.20	**1.33**	6.00	4.10	2.75	6.20	4.80	5.10
100-500	**2.28**	2.57	7.28	3.50	2.63	4.17	6.63	5.33
>500	4.00	4.00	5.28	**2.64**	4.57	4.07	4.40	5.60
Dimension d								
2	4.67	3.5	6.33	4.33	4.0	**2.83**	6.67	3.67
3-5	2.5	**2.21**	6.36	3.43	3.14	4.64	6.67	6.83
6-8	3.25	**2.5**	6.94	3.0	3.56	5.0	5.29	6.0
>8	**2.25**	3.75	6.31	3.19	2.5	5.19	5.29	4.19
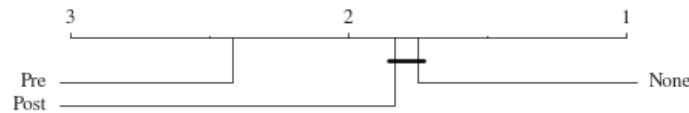
Figure 8. Performance of different rescalings

D.3. Canonical signature method

In Table 13 we give the full results for our canonical signature method on all UEA datasets, together with the results of Ruiz et al. (2020) used in Figure 6.

Finally, we give in Table 14 the hyperparameters that were selected for each dataset in the signature pipeline model.

Table 7. Accuracy of sensitivity-inducing augmentations per dataset

Dataset	Augmentation					
	None	Time	Basepoint	Invisibility-reset	Time + Basepoint	Time + Invisibility-reset
ArticularyWordRecognition	96.0	96.3	95.7	96.3	97.7	97.0
AtrialFibrillation	46.7	46.7	40.0	33.3	40.0	40.0
BasicMotions	100.0	100.0	100.0	100.0	100.0	100.0
CharacterTrajectories	88.3	93.2	86.4	88.7	93.8	93.7
Cricket	91.7	94.4	94.4	97.2	97.2	95.8
ERing	80.0	92.6	77.4	89.6	91.9	92.2
EigenWorms	72.5	79.4	74.8	76.3	87.0	81.7
Epilepsy	84.8	89.9	91.3	91.3	97.1	94.9
EthanolConcentration	27.8	29.3	33.5	41.8	34.6	41.4
FingerMovements	55.0	52.0	57.0	58.0	55.0	56.0
HandMovementDirection	29.7	33.8	32.4	33.8	36.5	32.4
Handwriting	21.9	30.8	23.6	24.6	30.6	28.7
JapaneseVowels	85.4	85.1	97.3	98.1	97.3	98.1
LSST	42.0	47.4	44.0	44.4	50.9	48.7
Libras	72.8	84.4	65.0	75.0	80.0	77.2
NATOPS	81.7	88.3	79.4	79.4	91.1	92.2
PenDigits	91.1	97.1	88.3	93.1	96.8	97.1
PhonemeSpectra	4.7	8.2	4.3	5.7	10.0	8.1
RacketSports	78.9	80.3	78.9	82.9	82.9	81.6
SelfRegulationSCP1	81.6	83.3	76.8	84.0	75.4	85.0
SelfRegulationSCP2	57.2	56.7	56.1	56.7	56.1	55.0
SpokenArabicDigits	82.5	85.5	80.5	88.0	85.1	90.1
StandWalkJump	60.0	46.7	40.0	46.7	40.0	46.7
UWaveGestureLibrary	84.1	87.5	79.7	82.8	87.5	83.4
Human Activity	73.0	76.6	92.3	92.2	93.0	93.8
Speech Commands	71.4	75.9	74.7	74.9	79.7	79.5
Average rank	4.69	3.12	4.87	3.29	**2.5**	2.54

Table 8. Accuracy of other augmentations per dataset

Dataset	Augmentation							
	None	Lead-lag	Coordinates projection			Random projection	Learnt projection	MHSP
			(1)	(2)	(3)			
ArticularyWordRecognition	97.7	96.3	83.3	95.7	97.0	95.3	73.7	80.3
AtrialFibrillation	46.7	40.0	53.3	53.3	46.7	66.7	46.7	53.3
BasicMotions	100.0	100.0	80.0	100.0	100.0	100.0	97.5	87.5
CharacterTrajectories	93.8	95.3	43.9	93.2	93.8	93.3	89.6	91.1
Cricket	97.2	98.6	90.3	97.2	95.8	88.9	69.4	56.9
ERing	92.6	94.8	79.3	89.3	91.9	74.4	62.2	61.1
EigenWorms	87.0	87.8	50.4	84.0	89.3	78.6	–	–
Epilepsy	97.1	97.1	55.8	95.7	95.7	81.9	67.4	65.9
EthanolConcentration	41.4	39.9	42.2	43.3	42.2	30.4	32.3	30.0
FingerMovements	56.0	–	59.0	58.0	–	55.0	60.0	65.0
HandMovementDirection	36.5	31.1	31.1	40.5	37.8	37.8	33.8	44.6
Handwriting	30.8	33.5	11.3	27.8	30.0	21.6	12.6	13.2
JapaneseVowels	98.1	97.6	94.1	97.8	97.6	84.1	95.4	95.9
LSST	50.9	55.6	43.5	51.7	52.8	43.7	34.4	39.8
Libras	84.4	86.7	47.8	83.9	85.0	86.7	73.3	81.1
NATOPS	92.2	–	33.3	90.6	91.1	85.6	83.9	81.7
PenDigits	97.1	98.3	60.2	96.8	97.2	96.7	96.5	97.4
PhonemeSpectra	10.0	–	4.5	9.4	10.6	8.9	7.2	7.7
RacketSports	82.9	82.2	53.3	85.5	84.2	75.7	73.7	75.0
SelfRegulationSCP1	85.0	86.0	61.8	85.0	84.0	81.6	86.7	84.6
SelfRegulationSCP2	56.7	57.2	55.6	58.9	55.6	60.6	59.4	57.8
SpokenArabicDigits	90.1	96.6	58.5	86.0	90.0	83.0	88.0	86.0
StandWalkJump	46.7	40.0	40.0	53.3	40.0	53.3	–	–
UWaveGestureLibrary	87.5	88.8	50.6	85.6	87.5	86.2	74.1	75.6
Human Activity	93.8	93.6	75.8	93.2	93.6	69.2	91.3	91.5
Speech Commands	79.7	–	14.9	77.1	–	70.2	–	76.1
Average ranks	2.9	**2.77**	6.52	3.33	3.23	4.71	5.83	5.31

Table 9. Accuracy of windows per dataset

Dataset	Window			
	Global	Sliding	Expanding	Dyadic
ArticularyWordRecognition	96.3	89.3	99.0	99.0
AtrialFibrillation	46.7	46.7	46.7	60.0
BasicMotions	100.0	100.0	100.0	100.0
CharacterTrajectories	93.2	94.6	96.9	97.1
Cricket	97.2	93.1	97.2	95.8
ERing	90.7	88.5	91.9	94.8
EigenWorms	80.2	74.8	78.6	76.3
Epilepsy	89.9	92.8	92.0	94.2
EthanolConcentration	30.4	38.8	30.0	35.7
FingerMovements	50.0	–	–	–
HandMovementDirection	33.8	33.8	36.5	33.8
Handwriting	30.1	21.5	30.2	27.2
JapaneseVowels	85.1	76.5	88.1	89.2
LSST	47.8	43.1	48.3	46.6
Libras	83.3	85.6	91.1	90.0
NATOPS	93.3	84.4	90.6	–
PenDigits	95.8	–	–	97.6
PhonemeSpectra	8.6	9.2	9.6	10.4
RacketSports	82.2	80.3	84.2	88.2
SelfRegulationSCP1	82.6	87.4	84.0	86.7
SelfRegulationSCP2	56.7	60.6	54.4	56.1
SpokenArabicDigits	85.5	91.5	93.7	96.6
StandWalkJump	46.7	53.3	46.7	53.3
UWaveGestureLibrary	86.6	79.4	89.1	89.7
Human Activity	76.1	73.0	80.4	81.7
Speech Commands	75.9	76.5	82.3	83.0
Average ranks	2.83	3.04	2.17	**1.73**

Table 10. Accuracy of signature and logsignature transforms per dataset.

Dataset	Transform	
	Signature	Logsignature
ArticularyWordRecognition	97.7	97.3
AtrialFibrillation	60.0	53.3
BasicMotions	100.0	100.0
CharacterTrajectories	93.8	93.8
Cricket	100.0	100.0
ERing	90.0	89.3
EigenWorms	79.4	81.7
Epilepsy	93.5	91.3
EthanolConcentration	31.9	30.0
FingerMovements	59.0	56.0
HandMovementDirection	40.5	40.5
Handwriting	35.3	24.5
JapaneseVowels	85.9	86.8
LSST	52.0	46.4
Libras	90.6	87.8
NATOPS	89.4	91.7
PenDigits	97.8	97.5
PhonemeSpectra	8.9	7.6
RacketSports	85.5	84.9
SelfRegulationSCP1	84.0	83.3
SelfRegulationSCP2	57.2	56.1
SpokenArabicDigits	87.5	85.8
StandWalkJump	53.3	53.3
UWaveGestureLibrary	90.0	86.9
Human Activity	78.7	78.3
Speech Commands	75.9	76.3
Average ranks	**1.25**	1.75

Table 11. Accuracy of rescaling choices per dataset

	Rescaling		
Dataset	None	Post	Pre
ArticularyWordRecognition	97.3	97.0	97.7
AtrialFibrillation	53.3	53.3	46.7
BasicMotions	100.0	100.0	100.0
CharacterTrajectories	94.6	94.6	94.6
Cricket	98.6	97.2	97.2
ERing	93.7	93.7	93.0
EigenWorms	80.9	80.9	79.4
Epilepsy	92.0	92.0	91.3
EthanolConcentration	31.2	31.6	30.0
FingerMovements	54.0	54.0	50.0
HandMovementDirection	35.1	32.4	29.7
Handwriting	36.6	36.4	37.1
JapaneseVowels	87.3	85.9	85.7
LSST	55.8	55.6	55.4
Libras	85.0	86.1	84.4
NATOPS	92.8	92.8	91.7
PenDigits	96.6	96.7	96.7
PhonemeSpectra	8.0	8.1	8.2
RacketSports	84.2	84.2	83.6
SelfRegulationSCP1	79.5	83.3	84.6
SelfRegulationSCP2	56.1	57.2	56.7
SpokenArabicDigits	90.5	90.5	90.2
StandWalkJump	46.7	53.3	46.7
UWaveGestureLibrary	87.5	87.2	87.2
Human Activity	85.0	84.6	85.1
Speech Commands	77.0	75.7	75.9
Average ranks	**1.73**	1.92	2.35

Table 12. Accuracy of (log)signature depth per dataset.

	Depth					
Dataset	1	2	3	4	5	6
ArticularyWordRecognition	83.3	96.0	97.3	97.7	95.3	–
AtrialFibrillation	40.0	40.0	60.0	33.3	40.0	53.3
BasicMotions	70.0	100.0	100.0	100.0	100.0	92.5
CharacterTrajectories	42.3	88.0	93.2	93.8	92.9	93.8
Cricket	30.6	93.1	97.2	98.6	100.0	–
ERing	77.0	89.6	90.0	89.3	88.9	84.8
EigenWorms	46.6	81.7	79.4	79.4	–	–
Epilepsy	50.7	78.3	89.9	93.5	93.5	93.5
EthanolConcentration	25.5	30.8	30.0	31.2	31.9	27.4
FingerMovements	57.0	58.0	59.0	–	–	–
HandMovementDirection	40.5	36.5	37.8	39.2	32.4	–
Handwriting	7.3	22.4	32.4	33.3	35.3	32.7
JapaneseVowels	78.9	85.9	86.8	84.3	81.4	–
LSST	40.9	45.6	47.6	50.6	52.0	44.7
Libras	51.7	77.2	85.0	87.8	88.9	90.6
NATOPS	35.0	86.7	91.7	–	–	–
PenDigits	60.0	90.4	96.9	97.7	97.4	97.8
PhonemeSpectra	4.1	7.6	8.9	–	–	–
RacketSports	44.1	77.0	78.9	84.9	85.5	82.2
SelfRegulationSCP1	53.6	80.2	84.0	83.3	81.9	–
SelfRegulationSCP2	56.1	55.0	56.7	54.4	57.2	–
SpokenArabicDigits	52.1	85.8	85.5	87.5	–	–
StandWalkJump	46.7	46.7	46.7	46.7	53.3	46.7
UWaveGestureLibrary	49.4	83.1	86.6	87.8	90.0	88.1
Human Activity	47.7	78.3	76.0	78.7	78.6	–
Speech Commands	14.8	69.6	76.3	–	–	–
Average ranks	4.73	3.44	2.62	2.48	**2.38**	3.04

Dataset	Classification method								
	DTWD	DTWA	DTWI	HIVE COTE	MLCN	MUSE	TapNet	gRSF	Signature Pipeline
ArticularyWordRecognition	98.7	98.7	98.0	99.0	95.7	99.3	95.7	98.3	97.7
AtrialFibrillation	20.0	26.7	26.7	13.3	33.3	40.0	20.0	26.7	46.7
BasicMotions	97.5	100.0	100.0	100.0	87.5	100.0	100.0	100.0	100.0
Cricket	100.0	100.0	98.6	98.6	91.7	98.6	100.0	98.6	95.8
Epilepsy	96.4	97.8	97.8	100.0	73.2	99.3	95.7	97.8	95.7
EthanolConcentration	32.3	31.6	30.4	79.1	37.3	47.5	30.8	34.6	43.3
ERing	91.5	92.6	91.9	97.0	94.1	97.4	90.4	95.2	94.8
FaceDetection	52.9	52.8	51.3	65.6	55.5	63.1	60.3	54.8	61.4
FingerMovements	53.0	51.0	52.0	55.0	58.0	55.0	47.0	58.0	52.0
HandMovementDirection	18.9	20.3	29.7	44.6	52.7	36.5	33.8	41.9	20.3
Handwriting	60.7	60.7	50.9	48.2	30.9	52.2	28.1	37.5	37.9
Heartbeat	71.7	69.3	65.9	72.2	38.0	71.2	79.0	76.1	69.8
Libras	87.2	88.3	89.4	90.0	85.0	89.4	87.8	69.4	93.9
LSST	55.1	56.7	57.5	57.5	52.8	64.0	51.3	58.8	56.9
NATOPS	88.3	88.3	85.0	88.9	90.0	90.6	81.1	84.4	92.2
PenDigits	97.7	97.7	93.9	93.4	97.9	96.7	85.6	93.5	97.4
Racketsports	80.3	84.2	84.2	88.8	84.2	92.8	87.5	88.2	90.8
SelfRegulationSCP1	77.5	78.5	76.5	85.3	90.8	69.6	93.5	82.3	78.8
SelfRegulationSCP2	53.9	52.2	53.3	46.1	50.6	52.8	48.3	51.7	50.6
StandWalkJump	20.0	33.3	33.3	33.3	40.0	26.7	13.3	33.3	46.7
UWaveGestureLibrary	90.3	90.0	86.9	89.1	85.9	93.1	90.0	89.7	90.9
Average Ranks	5.6	5.2	5.9	4.0	5.6	3.2	6.4	4.8	4.3

Table 13. Results of the signature canonical pipeline along with a selection of classifiers from Ruiz et al. (2020) (including the top performing MUSE algorithm) with a Random Forest for the UEA archive.

Dataset	Signature hyperparmeters		RF hyperparameters		Other
	Depth	Dyadic depth	Max depth	Num estimators	Training time (s)
ArticularyWordRecognition	2	2	45	500	60.3
AtrialFibrillation	1	2	None	50	35.9
BasicMotions	2	2	24	100	19.3
CharacterTrajectories	4	2	80	500	181.4
Cricket	2	4	6	500	249.0
DuckDuckGeese	1	2	16	100	140.9
ERing	2	3	8	1000	16.7
EigenWorms	3	3	12	100	250.1
Epilepsy	2	3	8	1000	42.8
EthanolConcentration	2	4	24	1000	454.2
FaceDetection	1	4	8	1000	1816.2
FingerMovements	1	2	4	100	30.8
HandMovementDirection	2	2	None	50	66.3
Handwriting	6	2	32	1000	280.3
Heartbeat	1	4	None	50	45.1
InsectWingbeat	1	3	45	1000	5367.5
JapaneseVowels	2	3	6	1000	95.4
LSST	4	2	60	1000	1590.5
Libras	6	2	None	100	28.4
MotorImagery	1	3	24	50	347.1
NATOPS	2	3	32	1000	37.8
PEMS-SF	1	3	80	1000	252.3
PenDigits	3	2	80	1000	302.3
PhonemeSpectra	2	4	45	1000	2188.7
RacketSports	3	2	None	500	13.9
SelfRegulationSCP1	3	2	None	100	186.6
SelfRegulationSCP2	3	2	6	50	138.1
SpokenArabicDigits	2	3	45	1000	1204.0
StandWalkJump	1	3	2	50	101.5
UWaveGestureLibrary	2	2	60	500	21.8

Table 14. Hyperparameters used for each dataset in the signature pipeline model.